Normalized Bispectrum Mapping for Probing Primordial Non-Gaussianity in Redshift Space

Master Thesis Project-II report submitted to

Indian Institute of Technology Kharagpur

in partial fulfilment for the award of the degree of

Integrated Master of Science

in

Physics

by

Aryabhatta Aryan

(20PH20005)

Under the supervision of

Prof. Somnath Bharadwaj

Department of Physics

Indian Institute of Technology Kharagpur

Spring Semester, 2024-25

April, 2025

DECLARATION

I certify that

(a) The work contained in this report has been done by me under the guidance of my supervisor.

(b) The work has not been submitted to any other Institute for any degree or diploma.

(c) I have conformed to the norms and guidelines given in the Ethical Code of Conduct of the Institute.

(d) Whenever I have used materials (data, theoretical analysis, figures, and text) from other sources, I have given due credit to them by citing them in the text of the thesis and giving their details in the references. Further, I have taken permission from the copyright owners of the sources, whenever necessary.

Date: April 30, 2025 (Aryabhatta Aryan)

Place: Kharagpur (20PH20005)

DEPARTMENT OF PHYSICS

INDIAN INSTITUTE OF TECHNOLOGY KHARAGPUR

KHARAGPUR - 721302, INDIA

CERTIFICATE

This is to certify that the project report entitled "**Normalized Bispectrum Mapping for Probing Primordial Non-Gaussianity in Redshift Space**" submitted by **Aryabhatta Aryan** (Roll No. 20PH20005) to Indian Institute of Technology Kharagpur towards partial fulfilment of requirements for the award of degree of Integrated Master of Science in Physics is a record of bona fide work carried out by him under my supervision and guidance during Spring Semester, 2024-25.

Date: April 30, 2025
Place: Kharagpur

Prof. Somnath Bharadwaj
Department of Physics
Indian Institute of Technology Kharagpur
Kharagpur - 721302, India

Abstract

Name of the student: **Aryabhatta Aryan** Roll No: **20PH20005**

Degree for which submitted: **Integrated Master of Science**

Department: **Department of Physics**

Thesis title: **Normalized Bispectrum Mapping for Probing Primordial Non-Gaussianity in Redshift Space**

Thesis supervisor: **Prof. Somnath Bharadwaj**

Month and year of thesis submission: **April, 2025**

The large-scale structure of the universe encodes invaluable information about the physics of the early cosmos, particularly through subtle deviations from Gaussianity in the primordial density fluctuations. This thesis advances the analysis and visualization of the bispectrum in redshift space-a higher-order statistical measure sensitive to three-point correlations in the matter distribution and a crucial probe of primordial non-Gaussianity (PNG). The study addresses the compounded complexity introduced by redshift space distortions (RSD), which arise from galaxy peculiar velocities and imprint anisotropies on observed clustering statistics. Building upon recent theoretical developments, the work implements a comprehensive computational framework that parameterizes triangle configurations in Fourier space using dimensionless variables and systematically maps the allowed configuration space. Interactive Python-based visualization tools are developed to render wavevector triangles, generate normalized bispectrum heatmaps, and explore the dependence of the bispectrum on triangle shape, orientation, linear bias, and PNG amplitude. The

methodology enables a detailed investigation of how different PNG templates-local, equilateral, and orthogonal-manifest in bispectrum measurements, and how RSD modifies these signatures. Results demonstrate that the bispectrum's configuration and orientation dependence, when accurately modeled, offer enhanced discriminatory power for constraining inflationary physics and cosmological parameters. The visualization platform developed herein facilitates intuitive exploration of these dependencies and supports future extensions to more complex cosmological scenarios. Overall, this research contributes both methodological innovations and physical insights, laying groundwork for improved interpretation of forthcoming large-scale structure surveys and advancing our understanding of the universe's initial conditions and subsequent evolution.

Contents

Chapter 1

Introduction

1.1 Introduction

Understanding the large-scale structure (LSS) of the universe is a central pursuit in contemporary cosmology. Over the past decades, progress in both observational campaigns and theoretical modeling has significantly advanced our comprehension of how the initial fluctuations from the early universe have evolved into the complex cosmic web observed today. These primordial fluctuations, generated during the inflationary epoch, are believed to be nearly Gaussian in nature. However, subtle deviations—collectively termed primordial non-Gaussianity (PNG)—encode vital information about the inflationary mechanism, including the field content, self-interactions, and non-linear dynamics that governed the early universe.

To probe these higher-order correlations, cosmologists rely on statistical measures that go beyond the two-point function. Chief among them is the bispectrum, the Fourier transform of the three-point correlation function, which captures the non-Gaussian features in the matter distribution. Unlike the power spectrum, which is insensitive to phase correlations and hence blind to non-Gaussianity, the bispectrum

is explicitly sensitive to the shapes and amplitudes of such deviations. Its configuration dependence enables discrimination among different PNG models, such as local, equilateral, and orthogonal types, which in turn are linked to distinct inflationary scenarios.

However, the extraction and interpretation of the bispectrum from observational data is complicated by redshift space distortions (RSD). Since galaxy redshifts contain contributions from both the Hubble flow and peculiar velocities along the line of sight, the inferred galaxy distribution in redshift space exhibits anisotropies not present in real space. These distortions manifest in two primary regimes: the Kaiser effect, which describes the coherent infall of galaxies into overdense regions on large scales, and the Finger-of-God effect, which results from small-scale random motions within virialized structures. Both contribute to angular-dependent modifications in clustering statistics, thus affecting bispectrum measurements.

When primordial non-Gaussianity and RSD are simultaneously considered, the redshift space bispectrum acquires a rich anisotropic structure. Specifically, the bispectrum becomes sensitive not only to the size and shape of the triangle formed by the three Fourier wavevectors but also to its orientation with respect to the line of sight. This anisotropy introduces additional degrees of freedom that, if modeled accurately, can provide constraints on the linear growth rate of structure, the strength of gravity on cosmological scales, and the PNG amplitude.

Recent efforts have aimed to formalize the parameter space of triangle configurations and develop computationally efficient tools for their visualization and analysis. In particular, the spherical harmonic decomposition of the redshift space bispectrum has emerged as a promising framework for quantifying its angular dependence. By isolating distinct multipole moments, this approach facilitates a more tractable comparison between theory and observations. Furthermore, interactive visualization tools—such as normalized bispectrum heat maps and triangle configuration

mappers—enable a comprehensive exploration of shape-dependent and orientation-sensitive features in the bispectrum.

1.2 Objective

The primary objective of this thesis is to advance the methodology for analyzing and visualizing the bispectrum in redshift space, with particular emphasis on the effects of primordial non-Gaussianity and redshift space distortions. This includes:

- Developing and applying computational tools for visualizing the allowed configurations of wavevector triangles and their orientation-dependent properties.
- Systematically exploring the theoretical framework connecting primordial non-Gaussianity, redshift space distortions, and higher-order statistics such as the bispectrum.
- Investigating the dependence of the bispectrum on key parameters, including the triangle shape, orientation, linear bias, and non-Gaussianity amplitude.
- Laying the groundwork for improved cosmological parameter estimation by accurately modeling and quantifying the anisotropic signatures in the bispectrum.

Through these objectives, this research aims to contribute to the broader understanding of the universe's large-scale structure, the physics of the early universe, and the interpretation of forthcoming large-scale structure surveys.

This introductory chapter establishes the conceptual framework and research motivation. The following chapters will review the foundational literature, describe the adopted methodology and computational strategies, present key results, and discuss their broader implications for cosmological inference.

Chapter 2

Literature Review

2.1 Large-Scale Structure and Cosmological Principles

The large-scale structure (LSS) of the Universe comprises a complex network of filaments, voids, walls, and clusters — collectively referred to as the *cosmic web*. These structures emerge from the gravitational amplification of initial density perturbations seeded during the inflationary epoch. In the simplest inflationary models, these fluctuations are modeled as Gaussian random fields; however, more general models predict small but significant deviations from Gaussianity.

To statistically describe the spatial distribution of matter, higher-order correlation functions are required. The bispectrum, being the Fourier counterpart of the three-point correlation function, is particularly sensitive to non-Gaussian features and plays a pivotal role in constraining the physics of the early Universe.

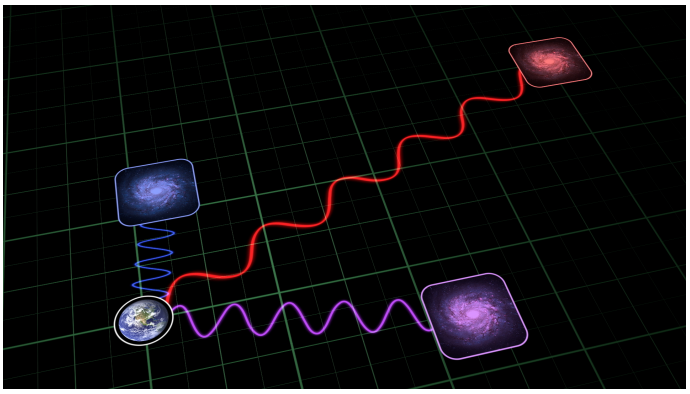

FIGURE 2.1: Redshift Space Distortion

2.2 Redshift Space Distortions (RSD)

In observational cosmology, galaxy positions are inferred via redshift, which includes both the cosmological expansion and peculiar velocities. This introduces distortions in the observed galaxy distribution:

- **Kaiser effect:** On large scales, coherent inflows into overdensities result in a squashing effect along the line of sight.
- **Finger-of-God (FoG) effect:** On small scales, random virial motions within collapsed halos produce elongation along the line of sight.

These effects cause the observed clustering to be anisotropic. While the power spectrum $P(k)$ remains a central tool for analyzing such data, it is blind to higher-order correlations and hence cannot capture non-Gaussian features.

2.2.1 Bispectrum in Redshift Space

The bispectrum in redshift space, $B_s(\mathbf{k}_1, \mathbf{k}_2, \mathbf{k}_3)$, depends on both the triangle configuration and its orientation with respect to the line of sight. A general triangle in Fourier space satisfies:

$$\mathbf{k}_1 + \mathbf{k}_2 + \mathbf{k}_3 = 0.$$

To analyze angular dependence, the bispectrum is decomposed in spherical harmonics:

$$B_s(\mathbf{k}_1, \mathbf{k}_2, \mathbf{k}_3) = \sum_{\ell,m} B^{\ell m}(k_1, k_2, k_3) Y_\ell^m(\hat{p}),$$

where $\hat{p}$ denotes the orientation of the triangle relative to the line of sight. Bharadwaj et al. show that, under linear theory and the plane-parallel approximation, only the even multipoles $\ell \leq 6$ with $|m| \leq 4$ contribute. This framework allows systematic extraction of redshift space anisotropies and their dependence on parameters like the linear growth rate f and non-Gaussianity amplitude $f_{\rm NL}$.

2.3 Primordial Non-Gaussianity (PNG)

Primordial non-Gaussianity arises from deviations in the initial conditions from pure Gaussian statistics, and it carries critical signatures of inflationary dynamics. The most widely studied PNG templates are:

Local Type

Dominant in squeezed configurations ($k_3 \ll k_1 \approx k_2$), modeled as:

$$B^{\rm local}(k_1, k_2, k_3) = 2 f_{\rm NL} \left[P_\phi(k_1) P_\phi(k_2) + \text{cyc.} \right]. \tag{2.1}$$

Equilateral Type

Maximized when $k_1 \approx k_2 \approx k_3$, represented by:

$$\frac{1}{6f_{\rm NL}} B_\Phi^{\rm equil} = -\left(P_1 P_2 + \text{cyc.}\right) - 2\left(P_1 P_2 P_3\right)^{2/3} + \left(P_1^{1/3} P_2^{2/3} P_3 + \text{cyc.}\right) \tag{2.2}$$

Orthogonal Type

A hybrid with flattened triangle sensitivity:

$$\frac{1}{6f_{\rm NL}} B_\Phi^{\rm ortho} = -3\left(P_1 P_2 + \text{cyc.}\right) - 8\left(P_1 P_2 P_3\right)^{2/3} + 3\left(P_1^{1/3} P_2^{2/3} P_3 + \text{cyc.}\right) \tag{2.3}$$

These templates are linked to different inflationary mechanisms, including multi-field models, non-canonical kinetic terms, or excited initial states. They imprint distinct scale-dependent bias signatures, especially in the halo power spectrum and bispectrum.

2.4 Cosmic Web Classification

The cosmic web is often classified using the eigenvalues of the tidal (or deformation) tensor:

$$T_{ij} = \partial_i \partial_j \Phi,$$

where Φ is the gravitational potential. Letting $\lambda_1 \geq \lambda_2 \geq \lambda_3$ denote the ordered eigenvalues, the classification is:

- **Void:** $\lambda_1, \lambda_2, \lambda_3 < 0$
- **Sheet:** $\lambda_1 > 0, \lambda_2, \lambda_3 < 0$
- **Filament:** $\lambda_1, \lambda_2 > 0, \lambda_3 < 0$
- **Knot:** $\lambda_1, \lambda_2, \lambda_3 > 0$

TABLE 2.1: Classification Scheme based on number of positive eigenvalues of T

Class	**Number of Positive Eigenvalues**	**Orbit Property**
Voids	0	Unstable Orbit
Sheets	1	1D stable manifold
Filaments	2	2D stable manifold
Clusters	3	Attractive fixed points

This dynamical classification connects local geometry to the anisotropic collapse behavior of matter and provides a useful framework for studying environmental effects on galaxy formation.

2.5 Computational Advances in Bispectrum Analysis

Recent advancements in numerical techniques have enabled efficient generation of non-Gaussian initial conditions for N-body simulations. Separable kernel-based methods facilitate rapid synthesis of complex bispectrum templates such as the equilateral and orthogonal types while preserving theoretical accuracy.

Interactive tools — such as triangle configuration mappers and normalized bispectrum heatmaps — have been developed to explore the parameter space of triangle shapes and orientations, enhancing both pedagogical and analytical utility.

2.6 Open Challenges

Despite significant progress, several challenges persist:

- **Non-linear RSD modeling:** Small-scale distortions require refined treatment via perturbation theory or effective field theory.
- **Degeneracy breaking:** Parameter degeneracies between $f_{\rm NL}$, linear bias, and RSD must be disentangled using joint analysis of multiple observables.
- **Survey systematics:** Observational effects such as selection bias, survey geometry, and shot noise must be carefully mitigated to enable robust PNG constraints.

These challenges motivate the development of precise modeling tools and visualization techniques, as presented in the subsequent chapters.

Chapter 3

Methodology

This chapter details the analytical and computational framework employed to parameterize, visualize, and analyze the bispectrum's dependence on triangle configurations and primordial non-Gaussianity (PNG). The methodology integrates theoretical derivations, valid configuration space mapping, and interactive visualization tools developed in Python Programming Language.

3.1 Theoretical Framework

3.1.1 Bispectrum Parameterization

Triangle Configuration in Fourier Space

The bispectrum is evaluated as a function of the triangle formed by three wavevectors $\mathbf{k}_1$, $\mathbf{k}_2$, and $\mathbf{k}_3$ in Fourier space, constrained by the closure condition:

$$\mathbf{k}_1 + \mathbf{k}_2 + \mathbf{k}_3 = 0.$$

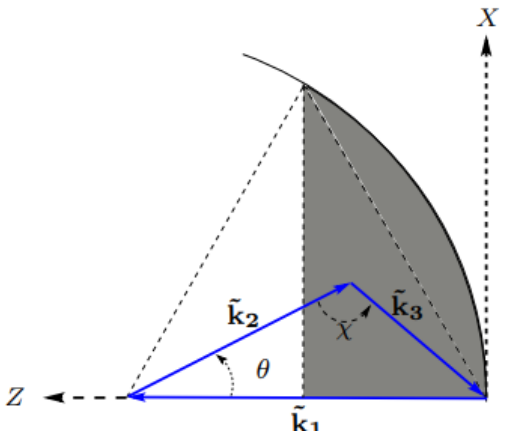

FIGURE 3.1: Wavevectors forming a triangle

To systematically explore triangle shapes, we adopt the following dimensionless parameters:

- **Shape parameter:**

$$t = \frac{k_2}{k_1}, \quad \text{with} \quad t \in [0.5, 1],$$

  which encodes the relative length of one triangle side.

- **Angle cosine:**

$$\mu = -\hat{\mathbf{k}}_1 \cdot \hat{\mathbf{k}}_2, \quad \text{with} \quad \mu \in [0.5, 1],$$

  representing the cosine of the internal angle between $\mathbf{k}_1$ and $\mathbf{k}_2$.

The allowed region in (μ, t) space is constrained by the triangle condition:

$$\mu \cdot t \geq \frac{1}{2},$$

ensuring that the third side k_3 is real and non-negative. Given (k_1, k_2, μ), the third side is computed via the law of cosines:

$$k_3 = \sqrt{k_1^2 + k_2^2 - 2k_1 k_2 \mu}.$$

This defines a triangular region in the (μ, t)-plane which uniquely maps to all triangle configurations up to rotation and scale. Notable triangle limits include:

- **Equilateral:** $t = 1$, $\mu = 0.5$,
- **Squeezed:** $t \to 1$, $\mu \to 1$,
- **Stretched:** $t \to 0.5$, $\mu \to 1$,
- **Flattened:** configurations near the boundary $t\mu = 0.5$.

Orientation Dependence

To describe orientation effects in redshift space, the triangle must be rotated with respect to the line-of-sight direction $\hat{\mathbf{z}}$. Let $p_z = \hat{\mathbf{k}}_1 \cdot \hat{\mathbf{z}}$ and $p_x = \hat{\mathbf{k}}_{1,\perp} \cdot \hat{\mathbf{z}}$, where $\hat{\mathbf{k}}_{1,\perp}$ is orthogonal to $\mathbf{k}_1$ in the triangle plane. The redshift-space bispectrum B_s can then be expressed as:

$$B_s(\mathbf{k}_1, \mathbf{k}_2, \mathbf{k}_3) = B_s(k_1, \mu, t, \hat{p}),$$

where $\hat{p} = (p_x, p_z)$ encodes the orientation of the triangle relative to the line of sight. This allows a spherical harmonic decomposition over triangle orientations:

$$B_s(k_1, \mu, t, \hat{p}) = \sum_{\ell,m} B^{\ell m}(k_1, \mu, t) Y_\ell^m(\hat{p}),$$

making the anisotropic structure of the bispectrum amenable to systematic analysis and visualization.

3.2 Computational Workflow

3.2.1 Parameter Space Mapping

To explore the bispectrum landscape, a discrete grid over the (μ, t) space was generated, satisfying:

$$0.5 \leq \mu \leq 1, \quad 0.5 \leq t \leq 1, \quad \mu \cdot t \geq 0.5.$$

For each point in this grid:

1. The triangle was reconstructed using the input (k_1, t, μ).
2. The corresponding k_2, k_3 was calculated.
3. The linear matter power spectra $P(k_i)$ were computed as:

$$P(k) = A_s \cdot k^{-3} \left(\frac{k}{k_0}\right)^{n_s - 1},$$

   where A_s is the amplitude, n_s the spectral index, and k_0 a pivot scale.
4. The bispectrum $B(k_1, k_2, k_3)$ was computed for each PNG type.
5. The normalized bispectrum (or reduced bispectrum) was computed as:

$$Q(k_1, \mu, t) = \frac{B(k_1, k_2, k_3)}{P(k_1)P(k_2) + P(k_2)P(k_3) + P(k_3)P(k_1)}.$$

3.3 Visualization Tools

To facilitate interpretation of the bispectrum across the triangle configuration space, a custom Python-based visualization tool, `TriPlot`, was developed. This tool was

designed to provide real-time interactivity and analytical insight into the dependence of the redshift space bispectrum on triangle shape and primordial non-Gaussianity.

The framework was implemented entirely in Python, leveraging several core libraries for numerical computation and visualization:

- **Matplotlib:** Used for generating static and interactive plots, rendering triangle geometries, and implementing GUI components such as sliders, buttons, and heatmaps.
- **NumPy:** Employed for efficient mathematical operations and array manipulations necessary for computing triangle side lengths, bispectrum values, and power spectra.

Together, these tools created a modular, extensible environment for visually and quantitatively exploring bispectrum behavior under various configurations and physical parameters. The visualization platform is structured to support future extensions, including integration with survey-specific geometry or advanced bispectrum templates.

Key Functionalities

The tool incorporates the following capabilities:

- Real-time triangle rendering from selected (μ, t) values in the configuration space.
- An interactive heatmap displaying the normalized bispectrum $Q(\mu, t)$ over the allowed region.

- Adjustable sliders for modifying key physical parameters: f_{NL}, k_1, and n_s.
- Support for switching between different primordial non-Gaussianity templates (local, equilateral, orthogonal).
- A color-coded overlay indicating the valid and invalid regions in (μ, t) space, based on triangle closure conditions.

This interactive tool enables a configuration-wise analysis of bispectrum sensitivity, aiding in the identification of triangle shapes and orientations where primordial signatures are most pronounced.

Chapter 4

Results and Discussion

This chapter presents the key findings from the bispectrum visualization and analysis framework developed in this study. Using the custom Python-based tool `TriPlot`, we systematically explored how triangle configurations and primordial non-Gaussianity (PNG) templates affect the structure of the redshift space bispectrum. Two main outputs are discussed: the real-time wavevector triangle rendering and the normalized bispectrum heatmaps across the (μ, t) parameter space.

4.1 Wavevector Triangle Visualization

The left panel of the visualization tool displays a reconstructed triangle formed by wavevectors $\mathbf{k}_1$, $\mathbf{k}_2$, and $\mathbf{k}_3$, based on the input parameters $t = k_2/k_1$ and $\mu = -\hat{\mathbf{k}}_1 \cdot \hat{\mathbf{k}}_2$. This provides geometric intuition into the shapes of bispectrum configurations.

Several characteristic configurations were explored:

- **Equilateral triangles** $(t = 1, \mu = 0.5)$: All sides equal. These configurations are especially sensitive to equilateral-type PNG.

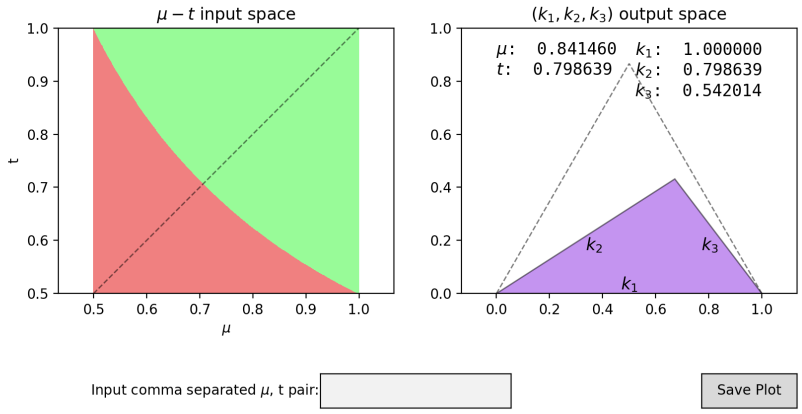

FIGURE 4.1: `TriPlot` - Visualizing triangle shapes for allowed μ-t space

- **Squeezed triangles** ($t \to 1, \mu \to 1$): One side much shorter than the other two. Local-type PNG peaks in this regime due to its divergence in the long-short mode coupling.
- **Flattened triangles** (boundary of $\mu \cdot t = 0.5$): Triangles that are nearly colinear. These are important for orthogonal PNG detection.
- **Stretched/elongated triangles** ($t \to 0.5, \mu \to 1$): Skewed shapes which help highlight shape-dependent suppression or enhancement in PNG.

4.1.1 Orientation Dependence

By projecting the triangle normal onto the line-of-sight (LoS) direction, the visualization reveals the anisotropic distortion introduced by redshift space effects. Coherent inflows or virialized motions alter the amplitude and symmetry of the bispectrum, depending on how the triangle is oriented.

Dynamic updates of triangle orientations (Fig. **??**) revealed that:

- **Anisotropy is most pronounced** for triangles aligned with the LoS, i.e., when the angle $\nu_1 \to 1$, indicating that the wavevector $\mathbf{k}_1$ is parallel to the

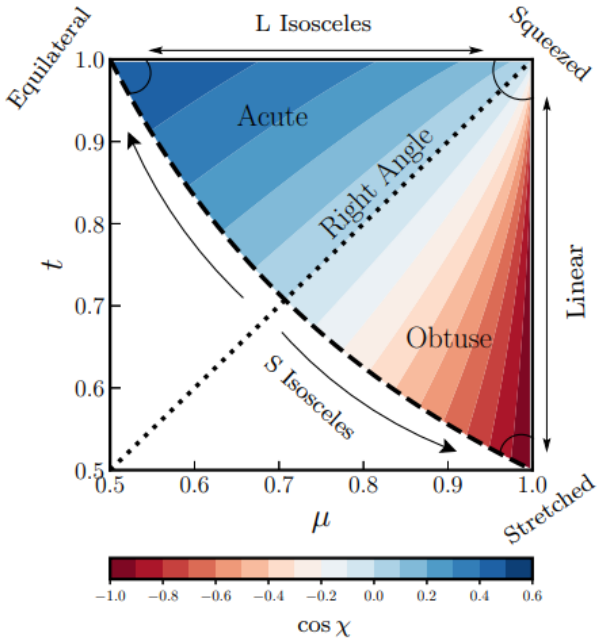

FIGURE 4.2: This shows the allowed μ, t space along with the triangle shapes corresponding to different values of μ and t

line of sight. These configurations are highly susceptible to redshift space distortions such as the Kaiser compression or Finger-of-God elongation.

- **Perpendicular orientations** ($\nu_1 \to 0$) exhibit minimal distortion, as expected under the linear Kaiser approximation. In this regime, the observed bispectrum closely reflects the real-space structure, allowing cleaner access to primordial features.

These orientation-dependent effects underscore the importance of modeling redshift space anisotropy accurately when interpreting bispectrum measurements from galaxy surveys. They also suggest that particular triangle orientations may enhance or suppress sensitivity to specific cosmological parameters, depending on the interplay between geometry and velocity-induced distortions.

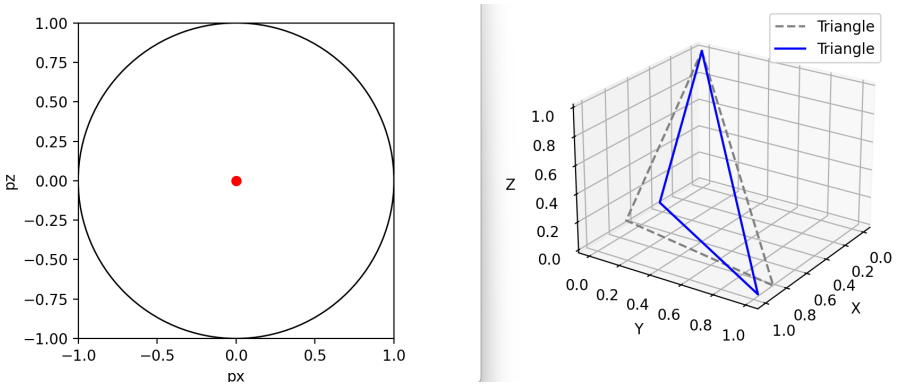

FIGURE 4.3: Visualizing orientation of triangles for varying $\hat{p}$

4.2 Normalized Bispectrum Heatmaps

The right panel of the tool displays the normalized bispectrum, or reduced bispectrum $Q(\mu, t)$, defined as:

$$Q(\mu, t) = \frac{B(k_1, k_2, k_3)}{P(k_1)P(k_2) + P(k_2)P(k_3) + P(k_3)P(k_1)},$$

evaluated across a dense grid in (μ, t)-space. Separate heatmaps were generated for each primordial non-Gaussianity template.

Key Observations

- **Local PNG:** As expected, the bispectrum exhibits strong enhancement in the squeezed limit ($\mu \to 1, t \to 1$). This reflects the divergent behavior of local PNG in long-short mode coupling. The heatmap shows a clear concentration of high-amplitude values in the upper-right corner of the valid triangle region.
- **Equilateral PNG:** The peak occurs around $(\mu, t) \approx (0.5, 1)$, corresponding to equilateral configurations. Suppression is seen in squeezed and stretched limits, consistent with theoretical expectations.

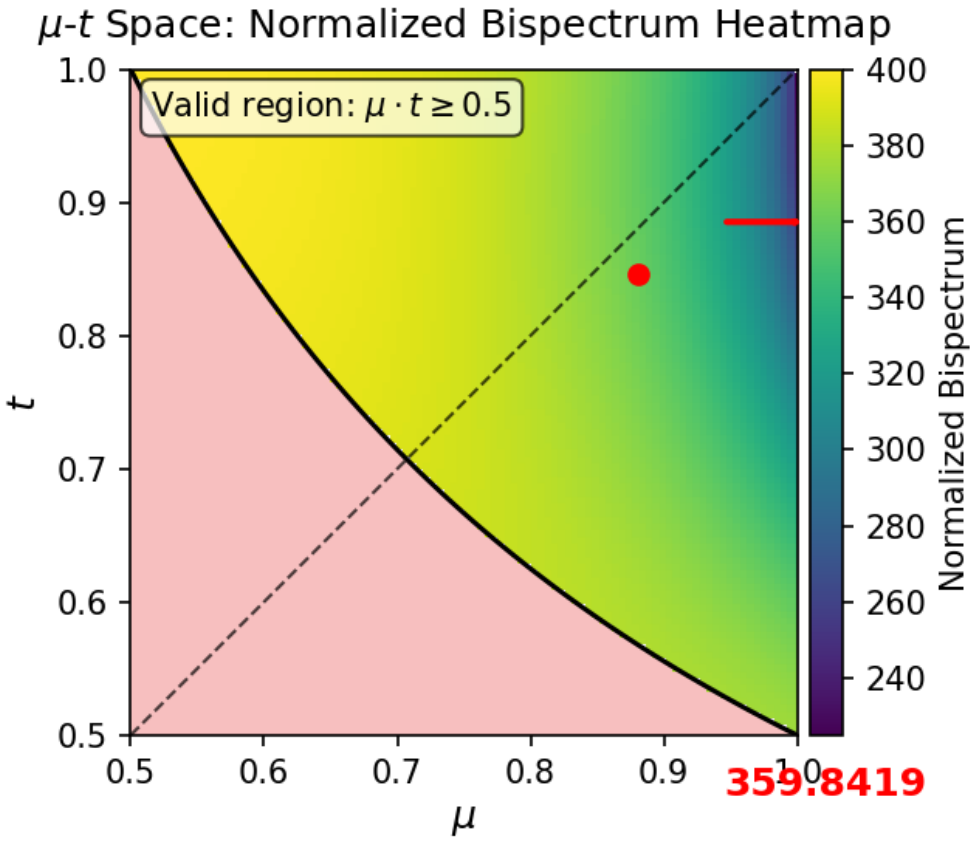

FIGURE 4.4: Heatmap of the normalized bispectrum $Q(\mu, t)$ for the orthogonal PNG template.

- **Orthogonal PNG:** The signal peaks along the boundary of the allowed region (flattened triangles), indicating sensitivity to configurations where $\mathbf{k}_3 \approx \mathbf{k}_1 + \mathbf{k}_2$. Orthogonal shapes help distinguish this template from the other two.

- **Continuity and Smoothness:** The heatmaps demonstrate smooth transitions between different regions of configuration space, indicating numerical stability of the bispectrum computation.

- **Normalized Range and Color Scaling:** Each heatmap was normalized independently, and invalid regions ($\mu \cdot t < 0.5$) were masked out. A boundary line is plotted to emphasize the allowed triangle space.

4.3 Physical Interpretation and Insights

These visualizations not only confirm known theoretical results but also provide an intuitive interface for exploring new questions:

- The (μ, t) parametrization is effective in collapsing a high-dimensional triangle space into a compact, interpretable domain.
- The bispectrum's sensitivity to triangle shape is highly non-linear, varying dramatically across different PNG templates.
- Orientation relative to the line of sight introduces additional anisotropy which, if not properly accounted for, may bias cosmological inference.
- The tool facilitates rapid hypothesis testing, such as identifying optimal configurations for maximizing PNG detectability in survey design.

The visualization outputs of `TriPlot` therefore offer not just confirmation of analytical results, but also an exploratory platform to intuitively understand the geometry-dependence of higher-order correlations in redshift space.

Chapter 5

Conclusion

5.1 Conclusion

This thesis has presented a systematic exploration of the redshift space bispectrum with an emphasis on its dependence on triangle configuration, primordial non-Gaussianity (PNG), and line-of-sight anisotropy. By integrating theoretical parameterizations with interactive computational tools, we have built a comprehensive framework for visualizing and interpreting the geometric and physical dependencies of the bispectrum.

A key contribution is the development of `TriPlot`, a Python-based visualization tool that enables real-time rendering of wavevector triangles and bispectrum heatmaps in the (μ, t) parameter space. Through this tool, we:

- Visualized canonical triangle configurations such as equilateral, squeezed, and flattened shapes, and linked them to PNG templates (local, equilateral, orthogonal).

- Explored anisotropic distortions induced by redshift space effects, confirming theoretical expectations regarding line-of-sight alignment and the Kaiser effect.
- Computed and analyzed the normalized bispectrum $Q(\mu, t)$ over the physically allowed triangle domain, identifying regions of peak signal for each PNG type.
- Verified theoretical scaling limits, such as the divergence of the local bispectrum in squeezed configurations, and assessed numerical stability through grid sampling and finite difference methods.

The combination of analytical modeling, efficient parameterization, and interactive visualization enables a powerful methodology for probing higher-order statistics in large-scale structure. This work supports not only conceptual understanding but also practical experimentation with cosmological models.

5.2 Future Prospects

The framework developed here opens up several avenues for future research and refinement:

- **Higher-Order Statistics:** While the bispectrum probes three-point correlations, further breaking of degeneracies in cosmological parameters—especially those involving bias, PNG, and growth rate—may require analysis of the *trispectrum*, the four-point correlation function in Fourier space. Future extensions of the current framework could enable:
  - Trispectrum shape classification in configuration space,
  - Joint bispectrum–trispectrum likelihood analysis,
  - Improved discrimination among inflationary models.

These future directions hold promise for deepening our understanding of cosmic structure formation and for extracting maximal information from next-generation cosmological datasets.

- **Machine Learning Integration:** With the increasing complexity and volume of cosmological data, machine learning techniques present a powerful opportunity. Neural networks can be trained to:
  - Rapidly estimate bispectrum amplitudes across large volumes of configuration space,
  - Automatically classify triangle shapes based on their information content,
  - Forecast parameter sensitivities for future surveys.

  These models could be particularly beneficial in speeding up likelihood evaluations in Markov Chain Monte Carlo (MCMC) pipelines for parameter inference.

- **Beyond Linear Theory:** While the current analysis is confined to the linear regime, future work can incorporate non-linear effects through the use of *Effective Field Theory of Large Scale Structure*. This would enable more accurate modeling of small-scale redshift space distortions, such as Finger-of-God effects, and non-linear mode-coupling between density and velocity fields.

- **Application to Mock Catalogs and N-body Simulations:** Applying the framework to synthetic galaxy catalogs would allow testing of detection thresholds, forecasting of survey sensitivity, and optimization of triangle selection strategies.

In summary, this thesis provides both a conceptual and computational foundation for the study of redshift space bispectra. With minor extensions, the methodology

is well-positioned to support precision cosmology efforts aimed at unraveling the physics of the early universe and the growth of structure on cosmic scales.

Bibliography

[1] Aryan, A. (2025). Triplot: Visualization tools for thesis project. `https://github.com/aryabhatta0/TriPlot-BispectrumViz-MTP`. Accessed: 2025-05-01.

[2] Bharadwaj, S., Mazumdar, A., and Sarkar, D. (2020). Quantifying the redshift space distortion of the bispectrum i: primordial non-gaussianity. *Monthly Notices of the Royal Astronomical Society*, 493(1):594–602.

[3] Forero-Romero, J. E., Hoffman, Y., Gottlöber, S., Klypin, A., and Yepes, G. (2009). A dynamical classification of the cosmic web. *Monthly Notices of the Royal Astronomical Society*, 396(3):1815–1824.

[4] Hahn, O., Porciani, C., Carollo, C. M., and Dekel, A. (2007). Properties of dark matter haloes in clusters, filaments, sheets and voids. *Monthly Notices of the Royal Astronomical Society*, 375(2):489–499.

[5] Inoue, S., Si, X., Okamoto, T., and Nishigaki, M. (2022). Classification of cosmic structures for galaxies with deep learning: connecting cosmological simulations with observations. *Monthly Notices of the Royal Astronomical Society*, 515(3):4065–4081.

[6] Mazumdar, A., Bharadwaj, S., and Sarkar, D. (2020). Quantifying the redshift space distortion of the bispectrum ii: induced non-gaussianity at second-order perturbation. *Monthly Notices of the Royal Astronomical Society*, 498(3):3975–3984.

[7] Peebles, P. (1993). *Principles of Physical Cosmology*. Princeton Series in Physics. Princeton University Press.

[8] Scoccimarro, R. (2000). The bispectrum: From theory to observations. *The Astrophysical Journal*, 544(2):597–615.

[9] Scoccimarro, R., Hui, L., Manera, M., and Chan, K. C. (2012). Large-scale bias and efficient generation of initial conditions for nonlocal primordial non-gaussianity. *Physical Review D*, 85(8).

[10] Wang, H., Mo, H. J., Yang, X., van den Bosch, F. C., and Jing, Y. P. (2012). Reconstructing the cosmic velocity and tidal fields with galaxy groups selected from the sloan digital sky survey. *Monthly Notices of the Royal Astronomical Society*, 420(2):1809–1826.